THE ASTROPHYSICAL JOURNAL, 425:L85–L88, 1994 April 20

COBE[1] DIFFUSE INFRARED BACKGROUND EXPERIMENT OBSERVATIONS OF GALACTIC REDDENING AND STELLAR POPULATIONS

R. G. ARENDT,[2] G. B. BERRIMAN,[3] N. BOGGESS,[4] E. DWEK,[4] M. G. HAUSER,[5] T. KELSALL,[4] S. H. MOSELEY,[4] T. L. MURDOCK,[6] N. ODEGARD,[3] R. F. SILVERBERG,[4] T. J. SODROSKI,[2] AND J. L. WEILAND[3]

Received 1993 August 26; accepted 1994 February 3

ABSTRACT

This *Letter* describes the results of an initial study of Galactic extinction and the colors of Galactic stellar populations in the near-IR using the Diffuse Infrared Background Experiment (DIRBE) aboard the *Cosmic Background Explorer* (*COBE*) spacecraft. The near-IR reddening observed by DIRBE is consistent with the extinction law tabulated by Rieke & Lebofsky (1985). The distribution of dust and stars in most of the first and fourth quadrants of the Galactic plane ($0° < l < 90°$, and $270° < l < 360°$, respectively) can be modeled as a stellar background source seen through up to ~ 4 mag of extinction at 1.25 μm. The unreddened near-IR colors of the Galactic disk are similar to those of late-K and M giants. The Galactic bulge exhibits slightly bluer colors in the 2.2–3.5 μm range, as noted by Terndrup et al. (1991). Star-forming regions exhibit colors that indicate the presence of a ~ 900 K continuum produced by hot dust or PAHs contributing at wavelengths as short as 3.5 μm.

Subject headings: dust, extinction — Galaxy: stellar content — infrared: stars

1. INTRODUCTION

The Diffuse Infrared Background Experiment (DIRBE) aboard *COBE* provides an important set of simultaneous observations of the Galaxy in 10 infrared (IR) bands. The full sky has been mapped with a $0.^\circ 7 \times 0.^\circ 7$ beam at wavelengths from 1.25 to 240 μm (Hauser et al. 1991; Boggess et al. 1992), with polarimetry from 1.25 to 3.5 μm (Berriman et al. 1993). The maps of the Galaxy at 1.25, 2.2, 3.5, and 4.9 μm clearly show a smooth Galactic disk of starlight surrounding a boxy elliptical bulge (Weiland et al. 1994, Fig. 1). At wavelengths of 12 and 25 μm, the stellar emission declines and the emission from warm dust in the interstellar medium (ISM) dominates the Galactic light (Fig. 1 [Pl. L6]). Extinction by dust in the ISM significantly influences the appearance of the Galaxy at 1.25 μm (e.g., a dust lane is visible across the bulge of the Galaxy), but it becomes less significant with increasing wavelength in accord with its known properties (e.g., Rieke & Lebofsky 1985). Sunlight scattered by dust within the ecliptic plane is visible with decreasing intensity at 1.25, 2.2, and 3.5 μm, while the same local dust contributes thermal emission over the 4.9–240 μm range, especially at 12 and 25 μm.

The DIRBE data offer the most complete IR survey of our Galaxy in terms of spatial and wavelength coverage. Previous large-beam near-IR investigations of the Galaxy (e.g., Matsumoto et al. 1982; Little & Price 1985; Kent et al. 1992) lacked the ability to exploit near-IR colors to examine and remove the effects of interstellar extinction, and to characterize stellar populations. The *Infrared Astronomical Satellite* (*IRAS*) surveyed diffuse emission only at wavelengths of 12 μm and greater, where thermal radiation from dust rather than starlight is the dominant emission. The DIRBE data allow investigation of the structure of the Galaxy through techniques not possible with either source counts (e.g., Whitelock & Catchpole 1992; Weinberg 1992) or previous infrared mapping (e.g., Blitz & Spergel 1991; Kent, Dame, & Fazio 1991).

This *Letter* examines the colors of the stellar populations and the characteristics of the interstellar extinction as observed in the near-IR (1.25–4.9 μm) DIRBE bands. Questions regarding the spatial structure of the stellar bulge and the disk of the Galaxy are addressed by Weiland et al. (1994), Freudenreich et al. (1993), Sodroski et al. (1994), and Dwek et al. (1994). Throughout this *Letter*, we use the term "intensity" to mean I_ν (shown as I for simplicity), and "color" to mean the ratio of intensities at two DIRBE wavelengths.

2. PHOTOMETRIC DATA

The photometric data used here consist of observations spanning the six month interval from 1989 December to 1990 June. The absolute calibration applied to the data from 1.25 to 12 μm was based on observations of Sirius. The flux density of Sirius was assumed to be 5740, 2440, 1090, and 595 Jy at 1.25, 2.2, 3.5, and 4.9 μm, respectively, based on the ground-based fluxes reported by Campins, Rieke, & Lebofsky (1985) and Rieke, Lebofsky, & Low (1985). The estimated systematic errors in the absolute calibration are $< 10\%$ between 1.25 and 4.9 μm; however, the errors in the ratios of intensities in adjacent bands are estimated to be $\lesssim 5\%$. All observations were interpolated to 90° solar elongation to remove the effect of elongation dependence on the zodiacal scattering and emission. Figure 1 shows DIRBE maps of the entire Galactic plane at 1.25, 2.2, 3.5, 4.9, 12, and 25 μm, with the interplanetary dust emission visible at wavelengths of 4.9 μm and longer where the ecliptic plane crosses the Galactic plane at $l \approx 0°$ and 180°. The brightness contributed by interplanetary dust scattering and emission was removed using an empirical fitting function (Hauser 1993). The estimated inaccuracy in the interpolation to 90° elongation and the removal of the interplanetary dust

[1] *COBE* is supported by NASA's Astrophysics Division. Goddard Space Flight Center (GSFC), under the scientific guidance of the *COBE* Science Working Group, is responsible for the development and operation of *COBE*.

[2] Applied Research Corporation, Code 685.3, NASA/Goddard Space Flight Center, Greenbelt, MD 20771.

[3] General Sciences Corporation, Code 685.3, NASA/Goddard Space Flight Center, Greenbelt, MD 20771.

[4] Code 685, NASA/Goddard Space Flight Center, Greenbelt, MD 20771.

[5] Code 680, NASA/Goddard Space Flight Center, Greenbelt, MD 20771.

[6] General Research Corporation, Technology Department, 5 Cherry Hill Drive, Suite 220, Danvers, MA 01923.

PLATE L6

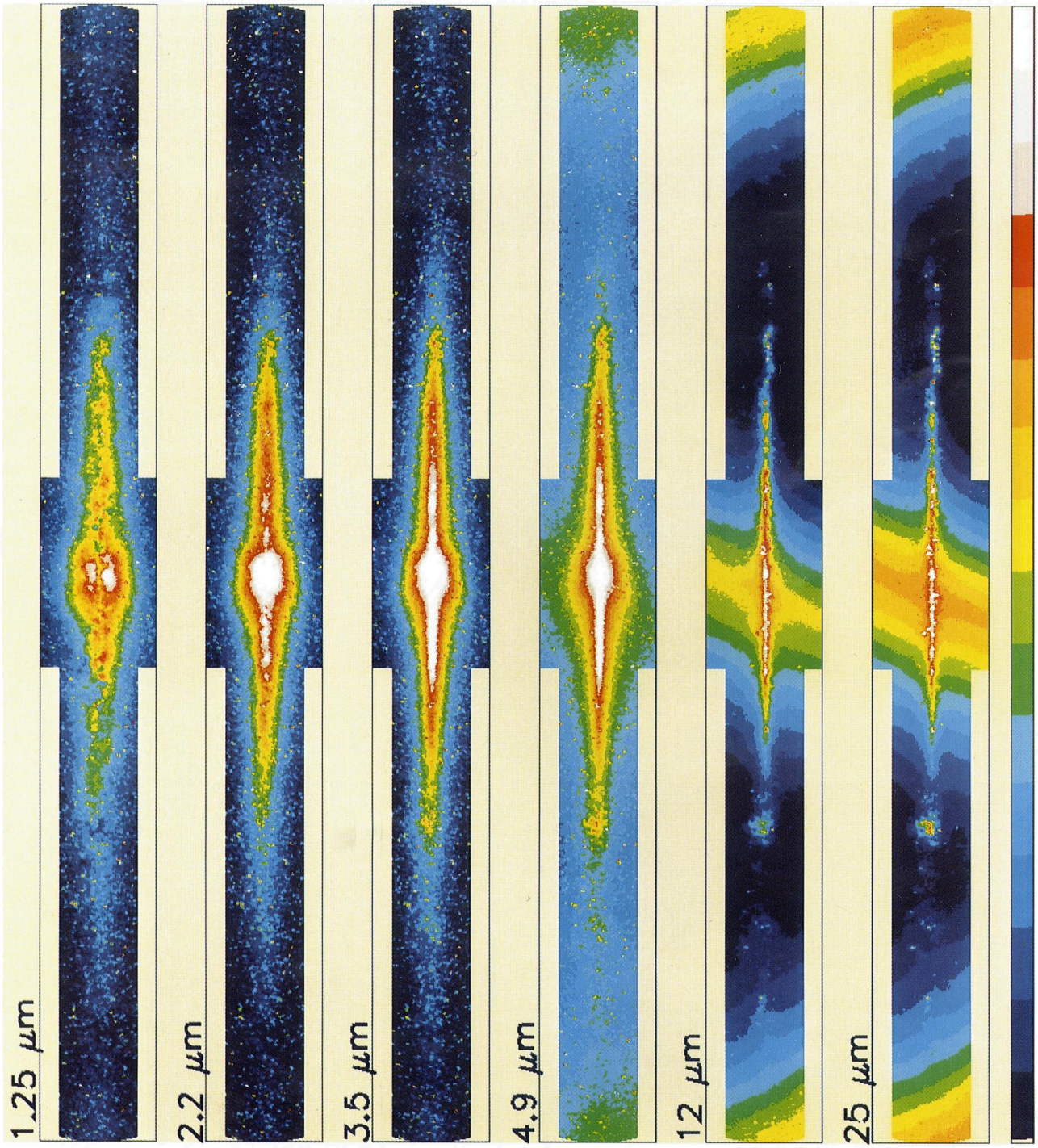

FIG. 1.—DIRBE images of the Galactic plane at 1.25–25 μm. Zodiacal emission is seen most prominently at 12 and 25 μm. The regions shown are from $l = +180°$ to $-180°$, and $|b| < 10°$ (or 15° for $|l| < 30°$). The solar elongation angle is 90° for all pixels. All images are on logarithmic scales ranging from $\log_{10}$ [I (MJy sr^{-1})] = [−0.2, 1.4] (1.25 μm); [−0.2, 1.4] (2.2 μm); [−0.4, 1.2] (3.5 μm); [−0.5, 1.1] (4.9 μm); [1.2, 2.0] (12 μm); [1.4, 2.2] (25 μm).

ARENDT et al. (see 425, L85)

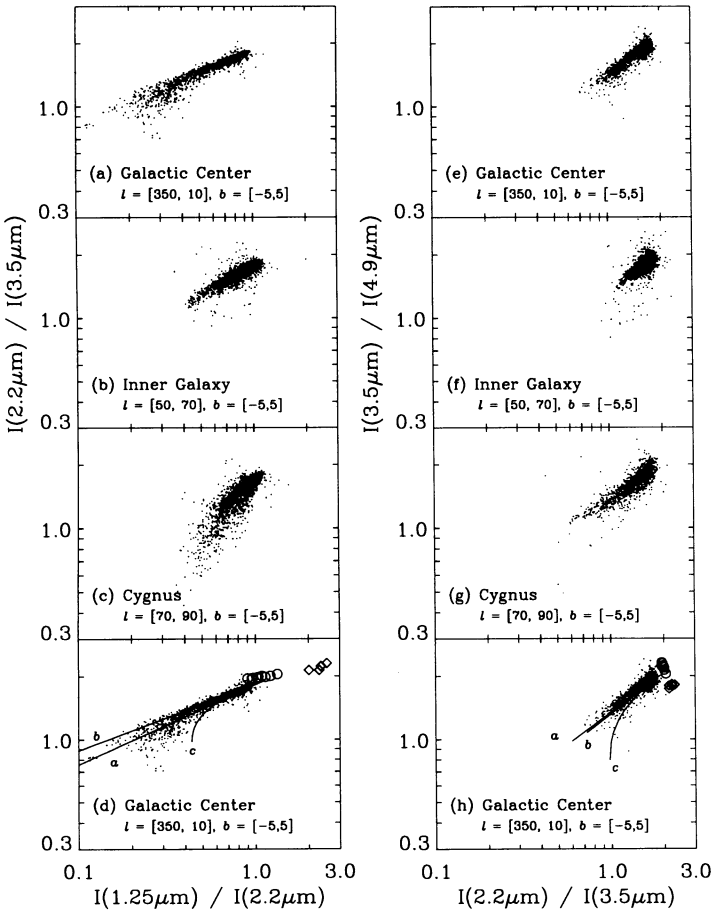

FIG. 2.—Near-IR color-color diagrams of Galactic emission: (*a*)–(*d*), short wavelengths; (*e*)–(*h*), long wavelengths. Each point plotted represents one (0°.32 × 0°.32) pixel. In Figs. 2*d* and 2*h* the circles and diamonds represent the observed colors of nearby stars (see § 4.1), and the lines indicate the effects of reddening for different geometries. See text for details.

foreground is $\lesssim 1\%$–2% (at 1.25–3.5 μm) and $\lesssim 5\%$ (at 4.9 μm) of the median brightness of the inner Galaxy. The errors in near-IR colors due to the combined uncertainties of the absolute calibration and the zodiacal emission subtraction are estimated to be $<10\%$. No color corrections were applied to the data, because the near-IR bands are relatively narrow.

3. REDDENING AND EXTINCTION

Color-color diagrams of $I(1.25\ \mu m)/I(2.2\ \mu m)$ versus $I(2.2\ \mu m)/I(3.5\ \mu m)$ and of $I(2.2\ \mu m)/I(3.5\ \mu m)$ versus $I(3.5\ \mu m)/I(4.9\ \mu m)$ were generated by plotting the intensity ratios of each DIRBE pixel (0°.32 × 0°.32) within various longitude ranges along the Galactic plane (Fig. 2). For the inner Galaxy ($|l| < 70°$), all three near-IR colors are linearly correlated with one another, implying that one parameter (e.g., amount of extinction) is sufficient to characterize the bulk of the observed color differences. The range of colors decreases towards the outer Galaxy (e.g., Figs. 2*a*, 2*b*, and 2*e*, 2*f*) and at higher latitudes. The range of colors is greatest for the $I(1.25\ \mu m)/I(2.2\ \mu m)$ color and decreases with increasing wavelength. In the fourth quadrant, at equivalent longitudes, the color-color diagrams appear very similar to those of the first quadrant.

In Figures 2*d* and 2*h*, the DIRBE-determined colors of nearby B- through M-type stars with low extinction are plotted for comparison with the integrated Galactic colors. The colors of the unreddened stars and the observed dispersion of Galactic colors suggest that interstellar reddening, rather than intrinsic variations of the stellar emission, is the dominant cause of color variations. The dispersion seen in the color-color diagrams for $|l| < 70°$ defines the reddening line for a single emitted spectrum seen through various amounts of extinction. The reddening has been quantified by comparison with reddening lines calculated in three different ways: (*a*) calculating a linear least-squares fit to the data with the assumption that all sources along a given line of sight are seen through the same amount of foreground extinction; (*b*) using published extinction laws (Koornneef 1983; Rieke & Lebofsky 1985; Mathis 1990) with the assumption of only foreground extinction (optical depth, $\tau_{1.25} = 0$–5); and (*c*) using the Rieke-Lebofsky extinction law assuming that the sources of emission (stars) and the absorbing medium (dust) are distributed uniformly along the line of sight.

The slopes of the reddening lines for various extinction laws, and as formally derived by a linear least-squares fit to the 1995 pixels plotted in Figures 2*d* and 2*h*, are listed in Table 1. The quoted errors represent the 10% uncertainty in the measured colors, and the variations found when fitting different subsets of the data. The DIRBE-derived reddening law (method [*a*]) most nearly resembles that implied by the Rieke-Lebofsky extinction law (method [*b*]). This similarity is enhanced if the fit is restricted to data where $\tau_{1.25} \lesssim 1$. Other tabulated extinction laws (e.g., Koornneef 1983; Mathis 1990) do not yield reddening that matches the DIRBE data as well, particularly in the redder colors. The least-squares fit and the Rieke & Lebofsky (1985) extinction law for both the foreground model and the intermixed model are plotted in Figures 2*d* and 2*h*. In the direction of the inner Galaxy and bulge ($|l| < 70°$, $|b| < 5°$), the reddening is too large and too liner to be caused by a mixture of dust and stars along the line of sight (method [*c*]), which is indicated by the curved lines in Figures 2*d* and 2*h*. With uniformly mixed dust and stars, the observed colors will

TABLE 1

SLOPES OF REDDENING LINES[a]

Source	$E(K-L)/E(J-K)$	$E(L-M)/E(K-L)$
This work ($\|l\| < 10°, \|b\| < 5°$)	0.38 ± 0.05[b]	0.62 ± 0.09[b]
Rieke & Lebofsky 1985	0.317	0.651
Mathis 1990	0.324	0.435
Koornneef 1983	0.258	0.412

[a] DIRBE bands at 1.25, 2.2, 3.5, and 4.9 μm correspond to the standard *J*, *K*, *L*, and *M* photometric bands, respectively.

[b] Uncertainties derived from uncertainties in color measurements, and variations in the sample selected for linear least-squares fitting.

always be dominated by relatively nearby unreddened emission. Apparently, toward the inner Galaxy, relatively distant sources dominate the observed emission despite higher extinction (at least 4 mag at 1.25 μm toward the Galactic center when averaged over the 0°.7 beam). The optical depths at 1.25 and 2.2 μm reach 1.0 within $\sim 3°$ of the Galactic plane at these longitudes (see § 4.2). This means that the different wavelengths used here will sample different path lengths in the Galactic plane, complicating any detailed analysis.

It is noteworthy that none of the simple reddening models used here adequately describe the color-color diagrams of star-forming regions like Cygnus. The Cygnus region ($l = 70°$–$90°$) shows a greater range of colors than suggested by the general trend of decreasing extinction with increasing longitude, and in the shorter wavelengths the trend has a significantly steeper slope (Figs. 2*c* and 2*g*). Possible explanations for this are discussed below (§ 4.4).

In principle, the reddening law we derive from the DIRBE data is not simply related to the true extinction law because the DIRBE observations may contain light scattered into the beam by the ISM in addition to the direct light of sources within the beam. The size of the effect will depend on the relative distribution of stars and dust, and on the optical properties of the dust grains. Simple estimates of the influences of scattered light indicate that its effects on the slope of the reddening line are too small to be apparent in this examination. This is supported by DIRBE observations of isolated stellar sources, which should not be affected by interstellar scattered light. A sample of such sources exhibits a reddening line consistent with that for the diffuse emission. In addition, light scattered by the ISM will result in an underestimate of the amount of extinction along a line of sight; however, simple estimates suggest that this effect is small. Throughout the remainder of this work we will therefore assume that the Rieke-Lebofsky extinction law adequately accounts for the reddening observed in the DIRBE data.

4. RESULTS AND DISCUSSION

4.1. *Colors*

The median colors of high latitude regions ($10° < |b| < 15°$) where the extinction appears to be low were used to define the nominal colors of Galactic stellar populations. For the bulge population such regions were at $10° > l > 350°$. Regions outside this longitude range were used to determine the nominal colors of the disk population. The extrapolation of the reddening lines from high-extinction regions (lower latitudes) passes through these median colors, supporting their choice as the nominal source population colors.

To characterize the integrated colors of the stellar populations, the nominal observed colors were compared with those of isolated bright stellar sources that were detected by DIRBE. In Figures 2*d* and 2*h*, K and M giants comprise the group of stars (indicated by circles) with redder colors, while the bluer group of stars consists of B3–F0 stars (indicated by diamonds). The unreddened Galactic light (from both bulge and disk) at 1.25–4.9 μm exhibits colors similar to those of late K and M giants. The bulge stars appear to have $I(2.2\ \mu\text{m})/I(3.5\ \mu\text{m})$ color $\lesssim 3\%$ bluer than the disk stars, which is in accord with the finding that the bulge stars are ~ 400 K hotter than their disk counterparts (Terndrup, Frogel, & Whitford 1991). Difficulty in accurately determining the limit of $\tau \to 0$ prevents clear distinction between the $I(1.25\ \mu\text{m})/I(2.2\ \mu\text{m})$ colors of the bulge and disk populations.

4.2. *Correlation of $\tau_{1.25}$ with τ_{240}*

Assuming that the Galaxy can be characterized by a single intrinsic $I(1.25\ \mu\text{m})/I(2.2\ \mu\text{m})$ color, the observed colors and the Rieke & Lebofsky extinction law can be used to construct a map of dust optical depth at 1.25 μm ($\tau_{1.25}$; Fig. 3*b* [Pl. L7]). A 5% difference in $I(1.25\ \mu\text{m})/I(2.2\ \mu\text{m})$ colors between bulge and disk would lead to an additive error of 0.08 in $\tau_{1.25}$. The extinction derived is a flux-weighted mean over the solid angle of the beam. Therefore, regions of high extinction that are smaller than the DIRBE beam are overlooked.

Toward the inner Galaxy and bulge, features in the $\tau_{1.25}$ map are anticorrelated with the intensity at 1.25 μm (Fig. 3*a* [Pl. L7]). The $\tau_{1.25}$ map has been compared with the optical depth map at 240 μm constructed from the dust emission in the 140 and 240 μm DIRBE bands under the assumptions of a single dust temperature along each line of sight and a λ^{-n}, $n = 2$, emissivity (Sodroski et al. 1993). Where $\tau_{1.25} \lesssim 1.0$, it is well correlated with the DIRBE 240 μm optical depth (Fig. 4), implying that where the line of sight is optically thin at 1.25 μm, the same dust is observed in both absorption and emission. The linear correlation of $\tau_{1.25}$ and τ_{240} breaks down along the Galactic plane, where $\tau_{1.25} > 1$ and $\tau_{240} \ll 1$, because the effective path length of dust sampled at 240 μm is longer than that at 1.25 μm. In regions toward the Galactic bulge where $\tau_{1.25} < 1.0$, the mean relation is $\tau_{240}/\tau_{1.25} = 0.0011$ for emissivity index $n = 2$, which is roughly $\frac{2}{3}$ of the value tabulated by Mathis (1990). For an emissivity index of $n = 1.5$, the derived dust temperature at 240 μm is higher, and $\tau_{240}/\tau_{1.25}$ is lowered by an additional factor of $\frac{2}{3}$.

4.3. *Extinction-corrected Galactic Maps*

The $\tau_{1.25}$ map can be used to correct for the effects of extinction on the DIRBE images of the Galaxy where the extinction is not too great ($\tau_{1.25} \lesssim 1$). The extinction-corrected intensity map, defined as $I_0(1.25\ \mu\text{m}) = I(1.25\ \mu\text{m}) \exp(\tau_{1.25})$, is shown in Figure 3*c* (Plate L7). Similar extinction-corrected maps can be generated for the other near-IR DIRBE bands, but the results are most dramatic at 1.25 μm where extinction is strongest. The extinction-corrected map shows a much smoother and more symmetric distribution of light from the

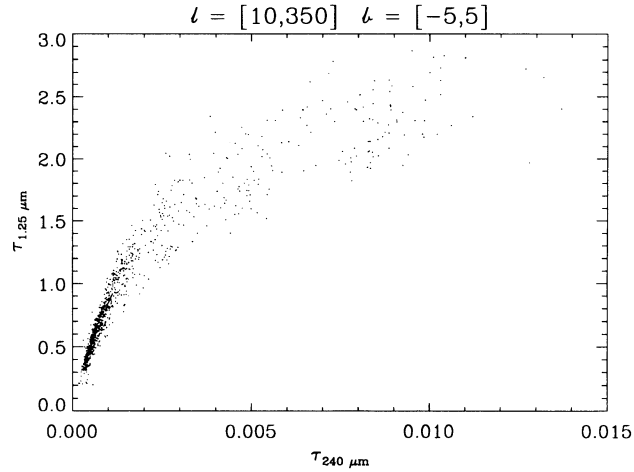

FIG. 4.—Correlation plot of optical depths at near- and far-IR wavelengths, $\tau_{1.25}$ vs. τ_{240}, for the region within 10° longitude and 5° latitude of the Galactic center. Where $\tau_{1.25} < 1.0$, the observed optical depths in the near- and far-IR are well correlated. At high optical depths, $\tau_{1.25}$ fails to sample the entire path length observed in the optically thin far-IR.

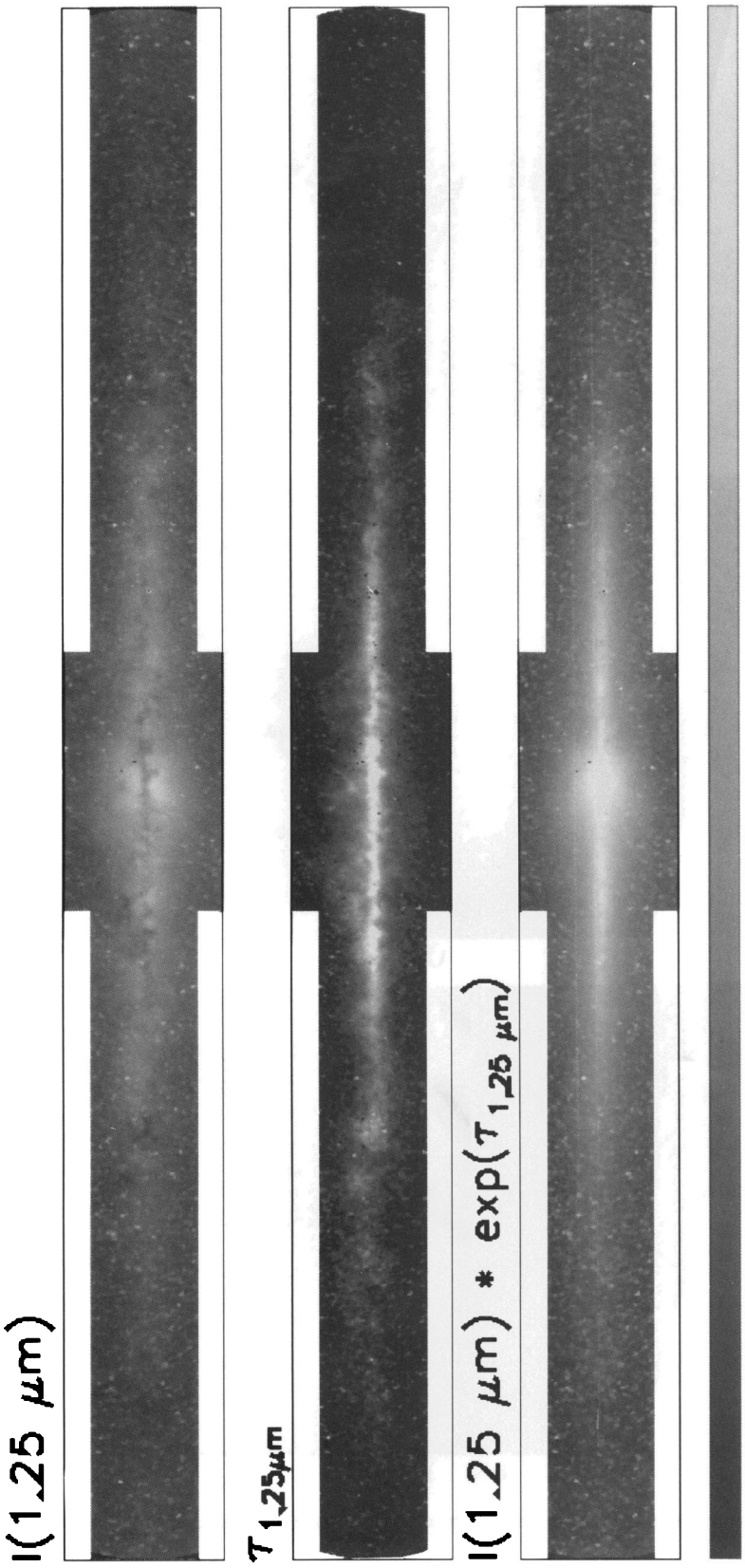

FIG. 3.—DIRBE images of (*a*) Galactic emission at 1.25 μm [I(1.25 μm)] with zodiacal light removed, (*b*) extinction at 1.25 μm ($\tau_{1.25}$), and (*c*) I_0(1.25 μm) with the effects of extinction removed [i.e. I(1.25 μm) * exp ($\tau_{1.25}$)]. Intensities are displayed on a logarithmic scale $\log_{10}$ [I (MJy sr^{-1})] = [−0.2, 1.5], and optical depths are displayed on a linear scale $\tau_{1.25}$ = [0, 2.5]. The extinction correction in Fig. 3*c* is not strictly valid in the Galactic plane where $\tau_{1.25} > 1$.

Galactic bulge and the inner Galaxy, allowing more accurate assessment of the structure of the inner Galaxy and bulge (Weiland et al. 1994). Once corrections for extinction are made, the differences in the Galactic structure across the four near-IR bands become much smaller (compare Figs. 3*c* and 1*c*). However, along lines of sight that ultimately reach high optical depths (e.g., $|b| \leq 3°$ toward the inner Galaxy), the most distant emission contributes negligibly to the observed emission, and thus the "extinction-corrected" maps cannot accurately represent the true emission that would be observed in the absence of interstellar extinction.

4.4. *Evidence for Near-IR Continuum Emission from Hot Dust*

The short-wavelength color-color diagrams of star-forming regions that are off the bright Galactic disk show a weaker correlation of colors with a steeper slope, than do the diagrams for the Galactic disk and bulge (Figs. 2*b*, 2*c*, and 2*d*). The slope is too steep to be created by reddening of starlight from a single population of stars. These star-forming regions (e.g., the Cygnus, Carina, and ρ Oph regions, Orion A and B, and the Rosette Nebula) are visible above the background confusion in the 3.5 and 4.9 μm bands, and correlate well with the bright sources seen in the 12 and 25 μm images.

Within the DIRBE near-IR bands there are no likely fine-structure, atomic hydrogen, or polycyclic aromatic hydrocarbon (PAH) lines that would be able to produce the observed color trends. The near-IR colors need to be explained by continuum emission. The apparently cool continuum which would be produced by the presence of several heavily reddened O stars (e.g., $\tau_{1.25} \approx 6$ or $A_v \approx 23$) in a typical star-forming region, could account for the energetics, but not the characteristic colors revealed in Figures 2*c* and 2*g*.

Continuum emission from dust or PAHs, however, can account for the observed colors. The shorter wavelength color-color diagrams for star-forming regions, as exemplified by the Cygnus region, can result from mixing the typical stellar emission of the Galactic disk with a second $\sim$900 K color temperature component arising only from star-forming regions. The longer wavelength color-color diagrams for star-forming regions can be interpreted in a similar fashion, except that here the color temperature of the second component appears to be $\sim$600 K. The tendency to see cooler temperatures with increasing wavelength is a natural result when the material actually emits over a broad range of temperatures.

If this near-IR emission of star-forming regions represents dust grains at equilibrium temperatures, the dust must lie very close to stars that cannot be resolved with the DIRBE beam. If the near-IR emission is due to continuum radiation from small, transiently heated grains or PAHs such as observed in reflection nebulae (e.g., Sellgren, Werner, & Dinerstein 1983; Sellgren 1984), then the dust or PAHs need not be so close to the stellar heating sources, and may appear diffuse with higher spatial resolution observations. More detailed analysis of the DIRBE data and future high resolution observations of specific star-forming regions is necessary for a thorough resolution of this phenomenon.

The authors gratefully acknowledge the efforts of the DIRBE data processing and validation teams in producing the high-quality data sets used in this investigation. We thank the referee for indicating potential systematic uncertainties in the analysis. We also thank C. Bennett and the rest of the *COBE* Science Working Group for helpful comments on this manuscript.

REFERENCES

Berriman, G. B., et al. 1993, ApJ, submitted
Blitz, L., & Spergel, D. N. 1991, ApJ, 379, 631
Boggess, N., et al. 1992, ApJ, 397, 420
Campins, H., Rieke, G. H., & Lebofsky, M. J. 1985, AJ, 90, 896
Dwek, E., et al. 1994, in preparation
Freudenriech, H. T., et al. 1993, ApJ, submitted
Hauser, M. G. 1993, in Back to the Galaxy (AIP Conf. Proc. 278), ed. S. S. Holt & F. Verter (New York: AIP), 201
Hauser, M. G., et al. 1991, in After the First Three Minutes, ed. S. S. Holt, C. L. Bennett, & V. Trimble (New York: AIP), 161
Kent, S. M., Dame, T. M., & Fazio, G. 1991, ApJ, 378, 131
Kent, S. M., Mink, D., Fazio, G., Koch, D., Melnick, G., Tardiff, A., & Maxson, C. 1992, ApJS, 78, 403
Koornneef, J. 1983, A&A, 128, 84
Little, S. J., & Price, S. D. 1985, AJ, 90, 1812
Mathis, J. S. 1990, ARA&A, 28, 37
Matsumoto, T., et al. 1982, in The Galactic Center, ed. G. Riegler & R. Blandford (New York: AIP), 48
Rieke, G. H., & Lebofsky, M. J. 1985, ApJ, 288, 618
Rieke, G. H., Lebofsky, M. J., & Low, F. J. 1985, AJ, 90, 900
Sellgren, K. 1984, ApJ, 277, 623
Sellgren, K., Werner, M. W., & Dinerstein, H. L. 1983, ApJ, 271, L13
Sodroski, T. J., et al. 1994, ApJ, in press
Terndrup, D. M., Frogel, J. A., & Whitford, A. E. 1991, ApJ, 378, 742
Weiland, J. L., et al. 1994, ApJ, 425, L81
Weinberg, M. D. 1992, ApJ, 384, 81
Whitelock, P. A., & Catchpole, R. M. 1992, in The Center Bulge, and Disk of the Milky Way, ed. L. Blitz (Dordrecht: Kluwer), 103